3D Printed Gyroid Lattices with Graded Density for Advanced Ballistic Protection

George Catalin CRISTEA*,[1], Mihail BOTAN[1], George PELIN[1], Adriana STEFAN[1], Alina DRAGOMIRESCU[1], Marian PATRASCOIU[2]

*Corresponding author
[1]INCAS – National Institute for Aerospace Research "Elie Carafoli",
B-dul Iuliu Maniu 220, Bucharest 061126, Romania,
cristea.george@incas.ro*, botan.mihail@incas.ro, pelin.george@incas.ro,
stefan.adriana@incas.ro, dragomirescu.alina@incas.ro
[2]Doctoral School of Biomedical Sciences, "Dunarea de Jos University",
111 Domneasca, Galati, Romania,
marian.patrascoiu@ugal.ro

DOI: 10.13111/2066-8201.2025.17.4.4

Received: 22 October 2025/ Accepted: 17 November 2025/ Published: December 2025

Abstract: *Additive manufacturing enables the fabrication of complex cellular architectures with controllable mechanical properties, making triple periodic minimum surface area (TPMS) networks promising candidates for lightweight, energy-absorbing applications. In this work, the mechanical response of 3D-printed polylactic acid (PLA) structures with gyroid filling was investigated under quasi-static compression and weight-drop impact. Three types of specimens with identical external dimensions (60 × 60 × 64mm) and comparable overall relative density (~26%) were fabricated: (i) uniform gyroid, (ii) a cell size graded variant, and (iii) a cell size graded variant plus wall. The relative density was experimentally verified by mass and geometric measurements, ensuring a fair comparison between the architectures. Mechanical tests focused on stress-strain behavior, stiffness, peak stress, and energy absorbed per unit volume. Impact tests were performed by free fall to evaluate the ability of each configuration to dissipate kinetic energy and to reveal possible sensitivity to strain rate. Particular attention was paid to the initiation and propagation of failure, as the studied architectures exhibit distinct collapse mechanisms. Preliminary observations suggest that functionally graded gyroid structures may provide better energy absorption compared to uniform grids. The motivation behind this research is the development of lightweight ballistic panels. Current ballistic protection systems are often limited by their high weight, which reduces mobility. By introducing grid structures based on gyroids with controlled relative density and functional grading, it is expected to achieve panels with reduced mass, while maintaining or improving energy absorption and impact resistance.*

Key Words: *Functional grading, energy absorption, lightweight structures, TPMS, relative density, ballistic panels*

1. INTRODUCTION

Lightweight vehicle protection is constrained by a permanent trade-off between weight and protection. Additive manufacturing (AM) cellular and metamaterial cores have emerged as a promising solution to change this trade-off by tailoring the deformation mode and specific

energy absorption (SEA) at a constant areal density or by increasing or decreasing the density in specific areas of interest. Within this class, triple periodic minimum surface area (TPMS) networks, especially the gyroid, exhibit smooth, shell-like loading trajectories, nearly uniform stress distributions, and favorable strength-to-weight ratios under compression and impact, making them attractive as energy-absorbing cores in sandwich armor and impact-attenuation panels. Recent reviews show the growing interest in AM networks for energy absorption and impact attenuation between polymers and metals, including their scalability and tunability through unit cell geometry and wall thickness. [1, 2].

A growing body of scientific work quantifies how TPMS networks outperform spar-based topologies in progressive crushing and SEA, and how functional grading (e.g., cell size and wall thickness variation) can further reduce peak loads while maintaining or increasing absorbed energy. Quasi-static and dynamic tests on gyroid/TPMS cores consistently show high SEA and stable collapse compared to conventional lattices; graded variants can increase energy absorption over uniform counterparts by up to ~30% at a similar relative density. [3, 4]. Beyond uniform designs, recent studies (experimental and numerical) demonstrate that gradation of the mesh through thickness allows spatial control of stiffness and plateau stress, providing lower transmitted peak force and improved load redistribution - properties directly relevant to backface deformation limits in armor systems. [5, 6].

For automotive ballistic applications, sandwich configurations combining a hard impact face with a lightweight architected core have demonstrated improved ballistic/impact performance at reduced mass, through impulse spreading and delayed localized failure. This trend is reported for both foams and architected cores and is increasingly being explored with AM TPMS meshes. Recent experimental/numerical studies of mesh/composite core sandwich armor subjected to ballistic or drop impact emphasize the dual design goals of lower peak force and shallower backface indentation at a constant surface density. [7 – 9].

This paper investigates three PLA lattices based on gyroids with the same global relative density but distinct internal architectures: a uniform gyroid (Gy), a cell size graded variant (GH), and a cell size graded variant plus wall (GTH). Quasistatic compression and low-velocity impact (drop weight impact) tests were performed to evaluate stiffness, initial modulus, peak and plateau forces, absorbed energy and SEA, permanent crush, and indentation depth. By comparing structures with approximately equal mass and volume, we isolate architectural effects on impact strength metrics, which are necessary for light vehicle protection. The results are discussed in the context of the literature on TPMS networks and functionally graded cores for impact and ballistic loading. [10 – 12].

2. MATERIALS AND METHODS

The objective of this study was to examine how different gyroid-based lattice architectures respond to quasi-static compression and low-velocity impact when manufactured at the same global relative density. To explore this, three distinct geometries were designed (Figure 1): Gy, GH, and GTH, each representing a different strategy for controlling the internal architecture of the lattice while preserving the same external dimensions (60×60×64 mm).

The first structure, Gy, served as the baseline. It features a uniform gyroid topology with constant cell size and constant wall thickness throughout its height. This design represents the most common gyroid implementation found in AM-based energy-absorbing cores.

The second structure, GH, introduces a functional gradient by varying the height of the cells along the Z-axis. Larger cells were placed at the bottom of the specimen, gradually transitioning to smaller cells toward the top. Despite this geometric variation, the wall

thickness remained constant. This approach allowed us to examine how modifying the local stiffness distribution affects global compression and impact behavior.

The third structure, GTH, combines both strategies by varying cell size and wall thickness along the height. In this specimen, cell dimensions decrease gradually from bottom to top, while the wall thickness increases over the same direction. This configuration creates a pronounced stiffness gradient and was expected to produce smoother load redistribution and more progressive collapse mechanisms.

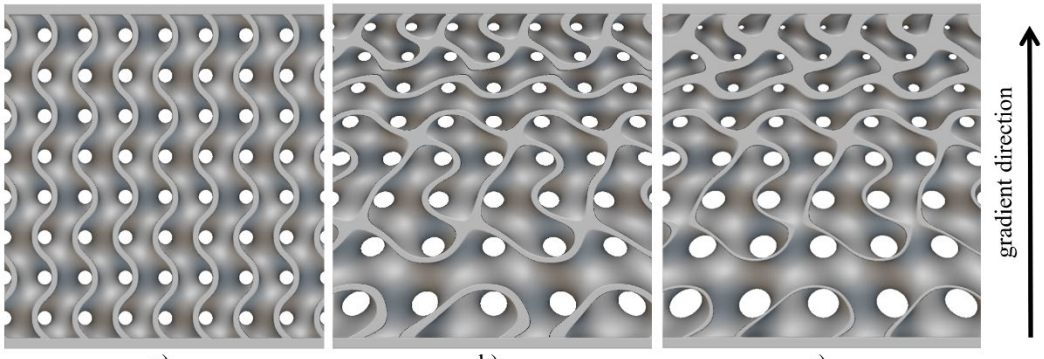

Fig. 1 - Geometric configurations of the three gyroid-based lattice architectures: (a) uniform gyroid (Gy); (b) cell-size graded gyroid (GH); and (c) combined cell-size and wall-thickness gradient (GTH)

All three architectures were generated with the explicit goal of maintaining the same overall mass, allowing the effect of internal geometry alone to be isolated and compared. The specimens were fabricated from polylactic acid (PLA) using a Bambu Lab P2S fused-filament fabrication system. PLA was selected not only for its ease of printing and dimensional stability, but also because it provides a consistent and reproducible platform for comparing geometric effects without additional complexities related to crystallinity or anisotropy. Printed specimens for each architecture are shown in Figure 2, confirming the geometric fidelity and consistency achieved through the chosen fabrication parameters.

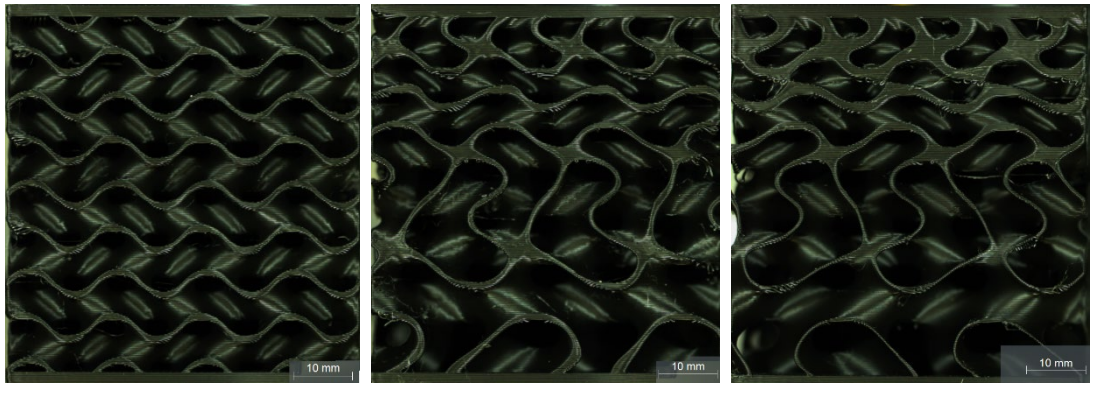

Fig. 2 - Photographs of the 3D-printed specimens for the three architectures. All samples were printed from PLA using identical process parameters to maintain equal relative density

To ensure uniformity across all architectures, the printing parameters were kept constant: layer height of 0.2mm, 0.4mm nozzle diameter, printing temperature of 220°C, bed temperature of 55°C, and vertical build orientation (Z-axis aligned with the gradient direction). Each specimen was printed as a single, monolithic body. Three replicates were produced for

each geometry, and their masses were measured immediately after fabrication. The resulting masses fell in a narrow range (76±1g), with variations below 0.15% across all geometries. This high level of repeatability ensures that the observed mechanical differences arise solely from architectural effects rather than density variations.

Since the goal was to compare architectural behavior at equal masses, the relative density of each sample was evaluated. The external volume of each sample (230.4cm³) was constant, so the relative density was calculated from the measured mass and the density of solid PLA (1.24g/cm³). All samples converged to a relative density of approximately 0.26, with differences between geometries within ±0.002. This small variation confirmed that any performance differences observed later were due to architectural effects, not mass differences.

To characterize the mechanical response under slow, controlled loading, all specimens were tested in compression using an Instron 5982 universal testing machine with the setup illustrated in Figure 3. The loading direction coincided with the build direction, allowing us to evaluate the collapse of the graded cores exactly as they would behave when integrated into a layered protective panel. A constant displacement rate of 5 mm/min was applied, and force–displacement data were recorded continuously. From each curve we extracted: the initial stiffness, determined from the linear region at small strains, the apparent modulus, based on geometry and measured stiffness, the peak force reached during collapse and the absorbed energy, computed as the area under the curve up to 20 mm displacement, a value chosen to represent moderate crushing while avoiding densification. After testing, each specimen was measured again to quantify permanent deformation and to document failure modes such as buckling, shear band formation, or asymmetric collapse.

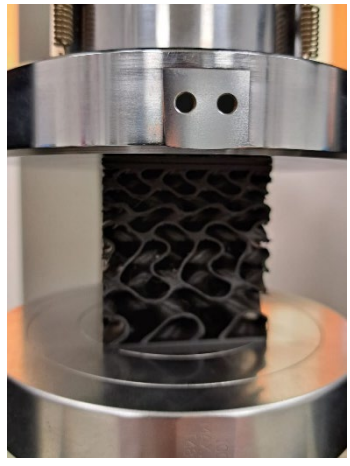

Fig. 3 - Quasi-static compression test configuration on the Instron 5982 machine, with loading applied along the build direction (Z-axis)

Dynamic response was assessed using a CEAST 9350 Drop Tower Impact System, operating at an impact energy of 50J. A 25mm spherical impactor was used to replicate localized impact conditions representative of practical loading scenarios in vehicle protection structures. Just as in compression, the impact direction was aligned with the gradient: from the stiffer, denser region toward the lighter, more compliant region. This configuration reflects how such lattice cores would be arranged in a ballistic or protective sandwich panel, where the denser region faces the incoming threat.

During impact, the system recorded time histories of force, energy, displacement, and velocity. From these curves we extracted: the maximum transmitted force, peak and total

displacement, the absorbed impact energy, the specific energy absorption (SEA) normalized by mass, and the crater depth formed on the impacted face. Following each test, specimens were visually inspected to identify perforation, cracking, delamination, or global collapse of the structure.

Integrations were performed with the trapezoidal rule, while mean and standard deviation were computed for all metrics across the three replicates.

3. RESULTS AND DISCUSSION

The mechanical and impact responses of the three gyroid-based network architectures reveal distinct deformation modes that arise solely from the internal geometry, as all specimens have nearly identical mass and relative density. The results highlight how subtle geometric gradations in cell size and wall thickness can dramatically alter the balance between stiffness, peak force, energy absorption, and residual deformation. Together, these behaviors are directly relevant to lightweight protective structures. Under quasi-static compression, the three architectures exhibited significantly different behaviors, as shown in Figure 4.

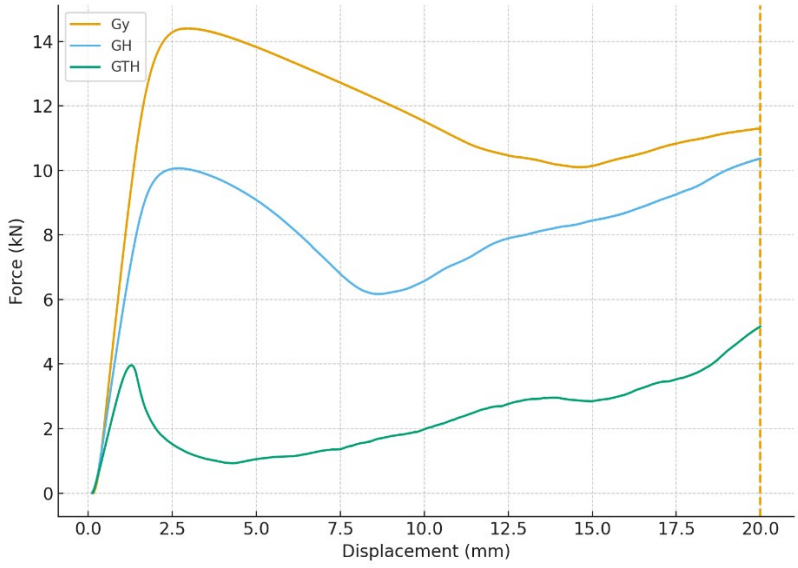

Fig. 4 - Force–displacement curves under quasi-static compression for the Gy, GH, and GTH architectures

The Gy structure, with its uniform cell and wall geometry, displayed the steepest initial slope and the highest load-carrying capacity. Its force-displacement curve rises rapidly and maintains elevated load levels up to the 20mm displacement considered here. The absorbed energy under compression was determined as the area under the experimental force–displacement curve up to a displacement of 20mm. Considering the discrete experimental points (Δ_i, F_i) with $\Delta_i \leq 20$mm, the absorbed energy U_{20} was obtained by numerical integration using the trapezoidal rule:

$$U_{20} = \sum_{i=1}^{m-1} \frac{F_i + F_{i+1}}{2} (\Delta_{i+1} - \Delta_i) \quad (1)$$

where F_i is the measured force (kN) and Δ_i is the displacement (mm). This generates a total absorbed energy of 226.4J, the highest among all specimens. Such behavior reflects a stiff,

load-bearing lattice that resists deformation but also transmits higher reaction forces which is an important consideration in applications where peak loading must be minimized.

The GH structure exhibited an intermediate response. By gradually reducing the cell size towards the top of the specimen, the load path becomes more flexible, allowing the structure to deform more progressively. The initial stiffness is lower than that of the Gy, and the force plateau is less pronounced, resulting in a total energy absorbed of 160.7J, approximately 29% lower compared to the Gy. Despite this reduction, the GH offers a smoother collapse and a more distributed deformation pattern, characteristics often desirable for impact mitigation, where progressive crushing is preferred over sudden load peaks.

The GTH structure showed the most flexible response because the lower thin-walled region yielded relatively quickly compared to the other architectures. The combination of decreasing cell size and increasing wall thickness towards the top significantly changes the stiffness distribution. The lower region, containing larger cells and thinner walls, acts as a sacrificial zone that begins to deform early, while the stiffer upper region engages later. This leads to a very slight increase in force and the lowest total energy absorbed, 47.2J, almost 80% lower than Gy. Although the structure deforms easily, its low resistance to compressive loading reduces its usefulness in scenarios where minimal structural stiffness is required. The integrated energy up to 20 mm displacement, summarized in Figure 5, highlights the strong architectural influence on crush resistance, with Gy absorbing nearly five times more energy than GTH.

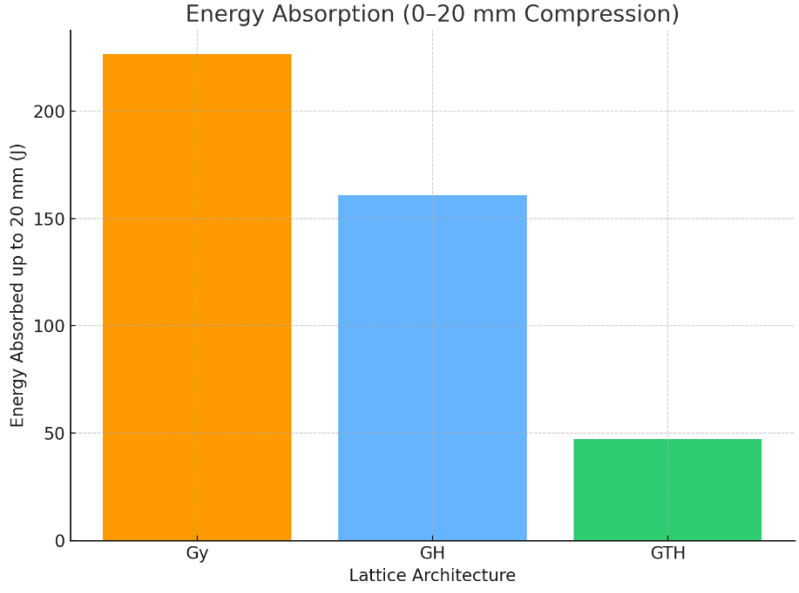

Fig. 5 - Comparison of the energy absorbed up to 20 mm displacement. The uniform Gy structure absorbs the highest energy, whereas the GTH structure shows substantially lower resistance to compression

Post-test measurements show permanent deformations consistent with the observed force-displacement behaviors. Gy retains a relatively uniform shape, with localized crushing distributed along the height, indicating a stable yet stiff collapse mode. GH displays a more progressive deformation, with the lower region (bigger cells) compacting earlier than the rest of the structure. GTH experiences substantial localized deformation in the lower region, where thin-walled, large-cell domains collapse early. This leads to a noticeable tilting or asymmetry in some samples, consistent with the structure's very low stiffness. These observations

reinforce the impact of internal grading: as stiffness gradients become more pronounced, deformation becomes increasingly localized.

The impact configuration shown in Figure 6 reproduces the expected load direction for protective cores, with the impactor striking the denser face first.

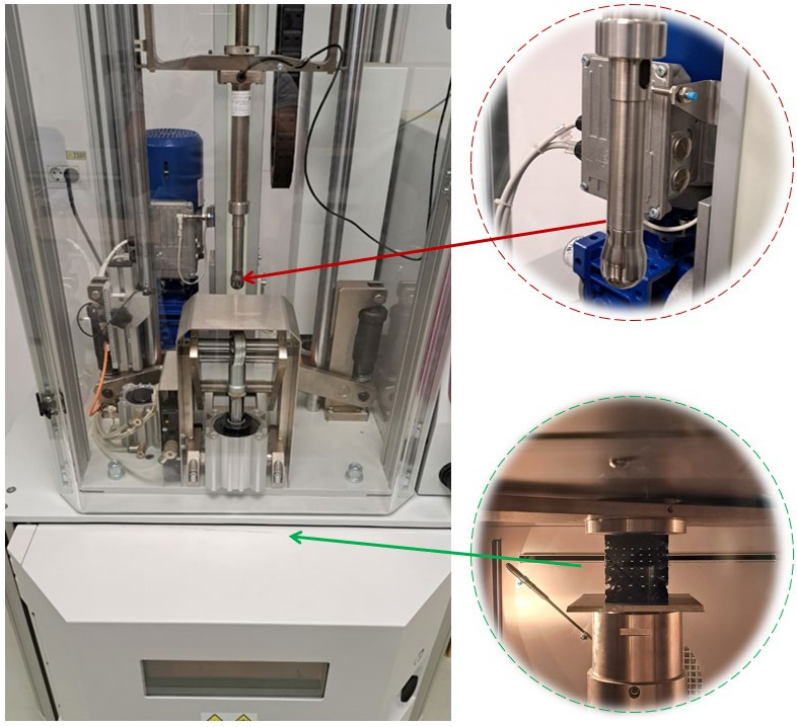

Fig. 6 - Experimental setup for low-velocity impact tests performed on the CEAST 9350 drop tower. The impact direction is from the denser region toward the more compliant region of the graded structures

Dynamic impact tests reveal behaviors that partially mirror quasi-static trends, but also highlight important differences due to speed sensitivity and localized loading. The GH structure produced the highest average peak force, approximately 7430N, consistent with its moderately stiff upper region resisting the incident impact. Interestingly, despite this high peak load, the GH exhibited the smallest crater depth (average 6.8mm), meaning that the deformation transmitted to the rear face was minimized. This suggests that the GH efficiently distributes the impact load throughout its thickness, reducing localized indentation. The Gy structure exhibited a lower peak force, approximately 6075N, but produced a significantly deeper crater, 10.1mm. This indicates that although the structure effectively absorbs energy, the uniform stiffness does not prevent local indentation. The Gy behaves like a stiffer spring under compression, but redistributes localized high-velocity loads less efficiently. The GTH structure produced the lowest peak forces, 5696N, and failed to puncture the upper surface because the structure failed from the lower density zone. Its global deformation was substantial and the structure tended to collapse through the lower weaker zone, resulting in large global displacements. This progressive collapse may be beneficial for reducing peak loads, but compromises the overall integrity under conditions of multiple impacts or repeated loading, which is undesirable in ballistic panels. The dynamic response shown in Figure 7 reveals clear differences in transmitted force. GH reaches the highest peak load, whereas GTH reduces the peak significantly due to its compliant lower zone. All specimens absorbed almost the entire

50 J input energy from the drop tower, but the way they dissipated this energy was different. Post-impact images in Figure 8 highlight the distinct failure modes: GH presents minimal face indentation, Gy shows deeper localized deformation, while GTH prevents perforation but collapses globally. The measured crater values for all tested specimens are presented in Table 1.

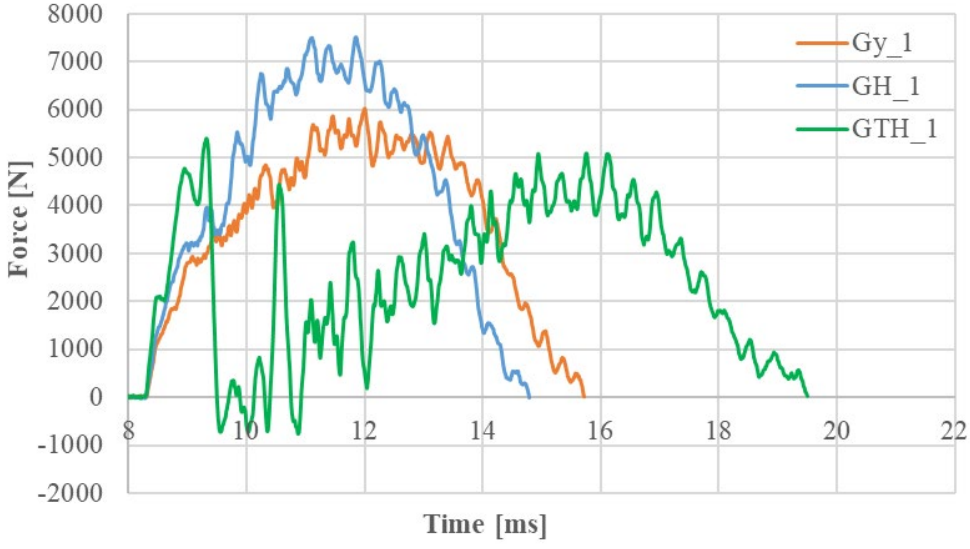

Fig. 7 - Representative impact force–time curves for the three lattice architectures. GH exhibits the highest peak force, while GTH shows the lowest transmitted peak

Gy GH GTH

Fig. 8 - Damage morphology and crater depth after impact. GH exhibits the shallowest crater, while GTH retains the upper face without perforation but undergoes extensive global deformation

When normalized by mass, the specific energy absorption (SEA) values converged to similar magnitudes (between 0.68 and 0.70 J/g), demonstrating that all three geometries are capable of dissipating the required impact energy when operating close to the failure threshold. The practical relevance, however, lies in the way the energy is distributed. Gy exhibits good SEA, but the deformation of the structure in the upper area is deeper. GH exhibits similar SEA, but with a reduced depth of the crater formed in the impact area and better localized load management. The GTH architecture also exhibits similar SEA, with a much lower peak force,

but this aspect becomes irrelevant when the overall structural stability is compromised. This highlights that the calculation of SEA alone is insufficient for the evaluation of energy absorption networks intended for ballistic or protective structures. The peak force, deformation mode and residual integrity are equally important.

Table 1 – Measured crater depths on the impacted face for the three lattice architectures

Architecture	Crater depth (mm)	Standard deviation (mm)	Remarks
Gy	10.06	0.31	Clear crater formation
GH	6.78	0.02	Shallow crater, localized deformation
GTH	0.74	0.02	No perforation, but compromised

Considering all static and dynamic mechanical indicators, the following trade-offs emerge: Gy offers the highest stiffness and compression energy absorption, but has moderate performance in localized impact due to deeper indentation; GH most effectively balances stiffness, peak load, and impact face deformation; while GTH excels in minimizing peak impact force, however, its reduced compressive stiffness and structural instability during impact reduce its suitability for armor applications requiring post-impact integrity.

5. CONCLUSIONS

This study investigated the compression and impact behavior of three gyroid lattice architectures: uniform (Gy), cell size graded (GH) and cell wall graded (GTH), fabricated by PLA filament and designed to have similar external dimensions and relative densities. The goal was to isolate the influence of internal architectural grading on energy absorption, deformation modes and dynamic response, with a view to their potential use in lightweight cores for automotive ballistic panels.

Under quasi-static compression, the three structures exhibited fundamentally different responses, despite an almost identical relative density. The uniform Gy lattice exhibited the highest stiffness and absorbed the most energy up to a displacement of 20mm (226J), but at the cost of higher transmitted forces and a steeper collapse. The GH structure demonstrated a more balanced mechanical profile, combining moderate stiffness with smoother, more progressive deformation and intermediate energy absorption capacity (161J), but also lower compressive force compared to the Gy architecture. In contrast, the GTH architecture, with its combined gradient in cell size and wall thickness, was the most flexible and exhibited early localized collapse, resulting in significantly lower compressive energy absorption (47J). Free-fall impact tests further revealed architectural distinctions. Although all structures dissipated almost the entire 50J impact energy, their deformation patterns and transmitted loads differed significantly. The GH network achieved the most favorable combination of reduced crater depth (approximately 6.8mm) and controlled deformation, despite exhibiting the highest peak force. The Gy structure produced a deeper indentation of the impacted face (approximately 10mm), indicating a less efficient redistribution of localized loads. The GTH structure, although it generated the lowest peak force and prevented perforation of the upper face, suffered extensive global collapse, reducing its suitability for applications requiring structural integrity after impact.

Overall, the results suggest that uniform cell size grading (GH) provides the most effective balance between stiffness, peak load management, deformation control and impact

attenuation, properties highly desired for lightweight protective structures. The uniform gyroid (Gy) remains effective in energy absorption, but would require additional restraints or facing layers to manage localized deformation. The combined graded structure (GTH) is advantageous for minimizing peak forces, but may be suitable in the case of optimizing the minimum wall thickness to avoid early failure.

These findings highlight the potential of functionally graded gyroid networks as tunable and architected materials for ballistic panels for next-generation vehicles, where the trade-off between mass, stiffness, and protective performance is critical.

Future work will extend this investigation to higher impact energies, alternative materials such as fiber-reinforced polymers, numerical simulations to optimize grading laws, and integration of graded gyroid cores into complete sandwich panel systems to evaluate their performance under realistic ballistic loads.

ACKNOWLEDGEMENT

This research was carried out within the framework of the Experimental Demonstration Project 126PED/ 2024, funded by the Executive Agency for Higher Education, Research, Development and Innovation Funding (UEFISCDI, Romania).

REFERENCES

[1] C. W. Isaac, and F. Duddeck, Current Trends in Additively Manufactured (3D Printed) Energy Absorbing Structures for Crashworthiness Application–a Review, *Virtual and Physical Prototyping*, 4 Volume **17**, 1058–1101, https://doi.org/10.1080/17452759.2022.2074698

[2] Y. Wu, J. Fang, C. Wu, C. Li, G. Sun, and Q. Li, Additively Manufactured Materials and Structures: A State-of-the-Art Review on Their Mechanical Characteristics and Energy Absorption, *International Journal of Mechanical Sciences*, Vol. **246**, 2023, p. 108102. https://doi.org/10.1016/j.ijmecsci.2023.108102

[3] Y. Lyu, T. Gong, T. He, H. Wang, M. Zhuravkov and Y. Xia, Study on the Energy Absorption Performance of Triply Periodic Minimal Surface (TPMS) Structures at Different Load-Bearing Angles, *Biomimetics*, Vol. **9**, No. 7, 2024. https://doi.org/10.3390/biomimetics9070392

[4] J. Noronha, J. Dash, M. Leary, M. Watson, M. Qian, E. Kyriakou and M. Brandt, Additively Manufactured Functionally Graded Lattices: Design, Mechanical Response, Deformation Behavior, Applications, and Insights, *JOM*, Vol. **75**, No. 12, 2023, pp. 5729–5754. https://doi.org/10.1007/s11837-023-06190-x

[5] N. Top, İ. Şahin and H. Gökçe, The Mechanical Properties of Functionally Graded Lattice Structures Derived Using Computer-Aided Design for Additive Manufacturing, *Applied Sciences (Switzerland)*, Vol. **13**, No. 21, 2023. https://doi.org/10.3390/app132111667

[6] A. Coluccia, G. Meyer, S. Liseni, C. Mittelstedt and G. De Pasquale, Functionally Graded Lattice Structures for Energy Absorption: Numerical Analysis and Experimental Validation, *Composite Structures*, Vol. **360**, 2025. https://doi.org/10.1016/j.compstruct.2025.119013

[7] S. Yang, C. Qi, D. Wang, R. Gao, H. Hu and J. Shu, A Comparative Study of Ballistic Resistance of Sandwich Panels with Aluminum Foam and Auxetic Honeycomb Cores, *Advances in Mechanical Engineering*, Vol. **2013**, 2013. https://doi.org/10.1155/2013/589216

[8] A. U. Haq and S. K. R. Narala, Experimental and Numerical Investigation on the Ballistic Impact Performance of Sandwich Panels with Additively Manufactured Honeycomb Cores, *Aerospace Science and Technology*, Vol. **155**, 2024, p. 109733. https://doi.org/10.1016/j.ast.2024.109733

[9] A. Jinnapat, P. Doungkom, K. Somton and K. Dateraksa, Ballistic Performance of Composite Armor Impacted by 7.62 Mm Armor Projectile, *Journal of Metals, Materials and Minerals*, Vol. **33**, No. 2, 2023, pp. 120–127. https://doi.org/10.55713/jmmm.v33i2.1698

[10] M. Overbeck, S. Heimbs, J. Kube and C. Hühne, Energy Absorption Properties of 3D-Printed Polymeric Gyroid Structures for an Aircraft Wing Leading Edge, *Aerospace*, Vol. **11**, No. 10, 2024. https://doi.org/10.3390/aerospace11100801

[11] J. Zhang, Y. Liu, B. Bahrami Babamiri, Y. Zhou, M. Dargusch, K. Hazeli and M.-X. Zhang, *Enhancing Specific Energy Absorption of Additively Manufactured Titanium Lattice Structures through Simultaneous Manipulation of Architecture and Constituent Material*, 2022.

[12] V. Shevchenko, S. Balabanov, M. Sychov and L. Karimova, Prediction of Cellular Structure Mechanical Properties with the Geometry of Triply Periodic Minimal Surfaces (TPMS), *ACS Omega*, Vol. **8**, No. 30, 2023, pp. 26895–26905. https://doi.org/10.1021/acsomega.3c01631